# Characterization of Stress Intensity Factors along an Interface Line Approaching the Vertex in Piezoelectric–Brass Bonded Joints

#### Chonlada Luangarpa

Faculty of Engineering, Thammasat School of Engineering, Thammasat University, 99 Village No.18 Phahonyothin Road, Khlong Luang, Pathum Thani 12121, Thailand lchonlad@engr.tu.ac.th (corresponding author)

## Hideo Koguchi

Niigata Institute of Technology, 1719 Fujihashi, Kashiwazaki City, Niigata 945-1195, Japan koguchi3@icloud.com

Received: 30 June 2025 | Revised: 22 July 2025 | Accepted: 2 August 2025

Licensed under a CC-BY 4.0 license | Copyright (c) by the authors | DOI: https://doi.org/10.48084/etasr.13076

#### **ABSTRACT**

In piezoelectric-metal bonded structures, stress singularities occur along the material interfaces due to mismatched mechanical and electromechanical properties. This study investigates the development of stress singularities along the interface line approaching the vertex in a three-dimensional bonded structure composed of piezoelectric ceramic layer (PZT-5H) and brass. The developed analytical model incorporates three-real singularity orders, capturing the intricate stress distribution near the junction corner. To characterize both the orders of singularity ( $\lambda_n$ ) and the corresponding stress intensity factors at different points along the interface, a combined numerical framework employing eigenvalue analysis and a conservative area integral is utilized. The results reveal clear variations in the intensity factors as the vertex is approached. The change in the intensity factor for each singular term is distinct, and the behavior deviates significantly from previously reported trends in single singularity cases. The correlation between the intensity factors at the vertex and along the interface line for multi-singularity cases remains unclear and requires further investigation. These findings contribute to a better understanding of the stress behavior in piezoelectric interfaces and offer a methodological foundation for analyzing other bonded structures involving multi-singularity terms.

Keywords-component; piezoelectric material; stress singularity; intensity factor; conservative integral

## I. INTRODUCTION

Piezoelectric bonded joints, such as those composed of PZT-5H and brass, are widely utilized in smart structures and microscale devices due to their unique electromechanical coupling behavior. However, owing to the mismatch in the material properties at the interface, these bonded systems exhibit stress singularities—particularly at geometric discontinuities, such as corners or edges. These singularities often serve as initiation sites for mechanical failure, especially under complex loading conditions [1-4].

Singular stress fields in piezoelectric bonded joints have been researched. Authors in [5] introduced the conservative integral for determining the intensity factors at vertices in bonded interfaces of 3D piezoelectric structures. In [6], the integral was extended to analyze the singularities along interface lines, establishing a more comprehensive view of the stress analysis in such systems. Authors in [7] emphasized the sensitivity of singular behaviors to the boundary conditions and interface geometry, employing a model that featured three

distinct singularity terms. The dominance of the vertex singularity was revealed, while significant stress was also highlighted along the interface line. The influence of the notch geometry has been examined, including anisotropic materials, adhesive configurations, and joint types under critical stress conditions [8–13].

Prior to the analysis of piezoelectric bonded joints, researchers in [14] conducted a study on the relationship between the singularities at the vertex and along the interface in 3D dissimilar material joints involving a single singularity. It was demonstrated that the intensity of the singular field along the interface increases toward the vertex, not involving piezoelectric materials. Moreover, the near-vertex stress behavior along the interface was shown to be expressible as a function of the vertex singularity itself. This conclusion has been validated for cases involving a single-order of singularity. However, for cases involving multiple singularity orders, such a relationship has not been clearly established.

The singularities in bimaterial wedges and notches were investigated in [15-18]. Numerical techniques for determining the  $\lambda_n$  and intensity factors in anisotropic or piezoelectric materials have since evolved, including eigenvalue methods and hybrid formulations [1, 2, 14, 19, 20]. These methods have formed the basis for contemporary modeling strategies in dissimilar material joints, influencing the present investigation.

The present study focuses on evaluating the evolution of stress singularities along a singular line in models that contain three singularity terms. In addition, the former aims to investigate whether the previously established relationship between the interface and vertex singularities remains valid in cases involving multiple singularities.

## II. METHODOLOGY

To analyze the singularity behavior in bonded systems, this study employs a numerical approach combining the eigenvalue analysis formulated via the Finite Element Method (FEM) and the conservative integral technique. The determination of the  $\lambda_n$  and their corresponding angular functions is carried out through an eigenvalue and eigenvector analysis. This approach builds upon the general formulation introduced in [21], and has been adapted to piezoelectric bonded interfaces in subsequent works [1, 2]. The conservative integral, based on a common concept described in [5-7], is employed to determine the intensity factors. This two-step strategy enables a detailed characterization of multi-term singularity fields in bonded piezoelectric systems.

#### A. Stress Singularity for Piezoelectric Bonded Interfaces

In this section, the fundamental equations describing the electromechanical interactions in piezoelectric materials are introduced [22]. The constitutive relationships are formulated by:

$$\sigma_{ij} = C_{ijkl} \varepsilon_{kl} - e_{kij} E_k \tag{1}$$

$$D_i = e_{kij} \varepsilon_{kl} + \chi_{ik} E_k \tag{2}$$

where (i, j, k, l = 1, 2, 3),  $\sigma_{ij}$  denotes the stress tensor,  $C_{ijkl}$  is the elastic stiffness constant,  $\varepsilon_{kl}$  represents the strain tensor,  $e_{kij}$  is the piezoelectric constant,  $E_k$  is the electric field component,  $D_i$  is the electric displacement vector, and  $\chi_{ik}$  is the dielectric permittivity constant. When body forces and free charges are neglected, the equilibrium equations take the form presented in:

$$\sigma_{ij,i} = 0, D_{i,i} = 0 \tag{3}$$

According to [5], asymptotic expansions are employed to characterize the stress fields near the singularity as shown in:

$$\sigma_{ij}(r,\theta,\phi) = \sum_{n=1}^{m} K_n \left(\frac{r}{l}\right)^{-\lambda_n} f_{ij}^{(n)}(\theta,\phi) \tag{4}$$

where  $(i, j = r, \theta, \phi)$ , r is the radial distance from the singular point, L is the representative model length,  $K_n$  is the stress intensity factor,  $f_{ij}$  represents the angular function, and m is the index for singularity terms.

The displacement components are:

$$u_i(r,\theta,\phi) = \sum_{n=1}^m K_n \left(\frac{r^{1-\lambda_n}}{t^{-\lambda_n}}\right) g_i^{(n)}(\theta,\phi)$$
 (5)

where  $u_i$  is the displacement in the i-th direction, and  $g_i$  represents the angular function of displacement.

Equations (4) and (5) are identical to those applicable to the non-piezoelectric materials. However, in the case of piezoelectric materials, the electrical effects must be considered. The electric displacement and potential near the singularity can be described asymptotically as indicated in:

$$\sigma_{4j}(r,\theta,\phi) = \sum_{n=1}^{m} K_n \left(\frac{r}{L}\right)^{-\lambda_n} f_{4j}^{(n)}(\theta,\phi)$$
 (6)

$$u_4(r,\theta,\phi) = \sum_{n=1}^{m} K_n \left(\frac{r^{1-\lambda_n}}{L^{-\lambda_n}}\right) g_4^{(n)}(\theta,\phi)$$
 (7)

where  $\sigma_{4j}$  is the electric displacement,  $u_4$  is the electric potential,  $f_{4j}$  is the angular function of the electric displacement, and  $g_4$  is the angular function of the electric potential. Based on the formulation proposed in [5], the unified singular expression incorporating three singular terms is given by:

$$[\boldsymbol{\sigma}(r,\theta,\phi)] = [\boldsymbol{f}(\theta,\phi)] \left[ \left(\frac{r}{L}\right)^{-\lambda} \right] [\boldsymbol{K}]$$
 (8)

where the terms of (8) are described by:

$$[\boldsymbol{\sigma}(r,\theta,\phi)] = \begin{cases} \sigma_{rr}(r,\theta,\phi) \\ \sigma_{\theta\theta}(r,\theta,\phi) \\ \sigma_{\phi\phi}(r,\theta,\phi) \\ \tau_{r\theta}(r,\theta,\phi) \\ \tau_{r\phi}(r,\theta,\phi) \\ \sigma_{\phi}(r,\theta,\phi) \\ \sigma_{r}(r,\theta,\phi) \\ \sigma_{\theta}(r,\theta,\phi) \\ \sigma_{\theta}(r,\theta,\phi) \\ \sigma_{\theta}(r,\theta,\phi) \end{cases}$$
(9)

$$[f(\theta, \phi)] = \begin{bmatrix} f_{rr}^{(1)}(\theta, \phi) & f_{rr}^{(2)}(\theta, \phi) & f_{rr}^{(3)}(\theta, \phi) \\ f_{\theta\theta}^{(1)}(\theta, \phi) & f_{\theta\theta}^{(2)}(\theta, \phi) & f_{\theta\theta}^{(3)}(\theta, \phi) \\ f_{\theta\phi}^{(1)}(\theta, \phi) & f_{\theta\theta}^{(2)}(\theta, \phi) & f_{\theta\phi}^{(3)}(\theta, \phi) \\ f_{\phi\phi}^{(1)}(\theta, \phi) & f_{r\theta}^{(2)}(\theta, \phi) & f_{r\theta}^{(3)}(\theta, \phi) \\ f_{r\theta}^{(1)}(\theta, \phi) & f_{r\theta}^{(2)}(\theta, \phi) & f_{r\theta}^{(3)}(\theta, \phi) \\ f_{\theta\phi}^{(1)}(\theta, \phi) & f_{r\phi}^{(2)}(\theta, \phi) & f_{\theta\phi}^{(3)}(\theta, \phi) \\ f_{\theta\phi}^{(1)}(\theta, \phi) & f_{\theta\phi}^{(2)}(\theta, \phi) & f_{\theta\phi}^{(3)}(\theta, \phi) \\ f_{4r}^{(1)}(\theta, \phi) & f_{4r}^{(2)}(\theta, \phi) & f_{4\theta}^{(3)}(\theta, \phi) \\ f_{4\theta}^{(1)}(\theta, \phi) & f_{4\theta}^{(2)}(\theta, \phi) & f_{4\theta}^{(3)}(\theta, \phi) \end{bmatrix}$$

$$[(10)$$

$$\left[ \left( \frac{r}{L} \right)^{-\lambda} \right] = \begin{bmatrix} \left( \frac{r}{L} \right)^{-\lambda_1} & 0 & 0 \\ 0 & \left( \frac{r}{L} \right)^{-\lambda_2} & 0 \\ 0 & 0 & \left( \frac{r}{L} \right)^{-\lambda_3} \end{bmatrix}$$
(11)

#### B. Numerical Procedure

The numerical procedure is based on the method proposed in [5], consisting of two key steps. First, the  $\lambda_n$  and the corresponding angular functions are determined using the eigenvalue analysis based on the FEM. Second, the  $K_n$  are computed using the conservative integral. These two stages provide a comprehensive framework for evaluating the singular stress behavior in piezoelectric bonded joints.

#### C. Analytical Model

This study analyzes a three-dimensional bonded joint consisting of a PZT-5H and a brass substrate, subjected to compressive loading. The poling direction of the piezoelectric layer is normal to the interface. Details of the geometry and boundary conditions are presented in Figure 1. The bottom surface is fixed, and 1 MPa compressive load is applied to the top.

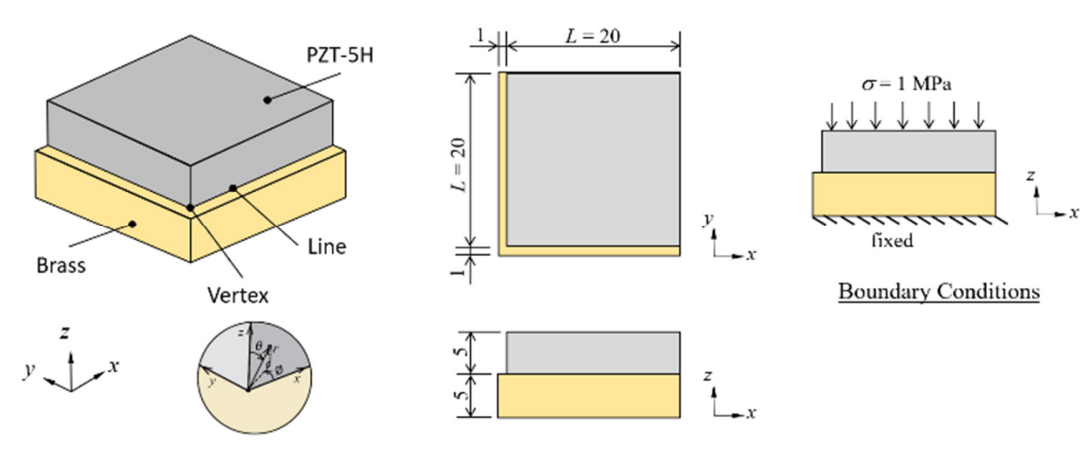


Fig. 1. Analytical model and boundary conditions.

The materials used in [7] are adopted in this study, with their mechanical and piezoelectric properties listed in Table I.

TABLE I. MECHANICAL AND PIEZOELECTRIC PROPERTIES

Material	Symbol	PZT-5H	Brass
Elastic constant (GPa)	$C_{11}$	126	
	$C_{12}$	55	E = 100  GPa and $v = 0.307$
	$C_{13}$	53	
	$C_{33}$	117	and $v = 0.307$
	$C_{44}$	35.3	
Piezoelectric constant (C/m²)	e <sub>31</sub>	-6.5	
	e <sub>33</sub>	23.3	
	$e_{15}$	17.0	
Dielectric constant (10 <sup>-10</sup> C/Vm)	χ11	151	
	χ33	130	

Prior to the detailed investigation of the singular behavior at the bonded vertex, an initial FEM simulation was performed using MSC Marc to examine the mechanical stress and electric displacement distributions. A refined mesh was generated in the vicinity of the vertex to capture the localized field variations accurately. The model consists of 49,988 eight-node brick elements with a total of 52,028 nodes. To capture the localized field variations near the singular region with sufficient accuracy, a refined mesh was applied in the vicinity of the vertex, where the smallest element width is less than 0.001 mm. Figure 2 presents the magnified views of the normal stress  $(\sigma_{\theta\theta})$  and electric displacement  $(D_{\theta})$  near the vertex region, respectively. These figures indicate that the region surrounding the vertex exhibits significantly higher stress and electric displacement magnitudes compared to the surrounding

areas. Elevated values are also observed along the interface line.

## D. Order of Singularity and Angular Functions Determination

The  $\lambda_n$  is evaluated through an eigenvalue analysis framework implemented via the FEM. Detailed formulations for three-dimensional joints can be found in [21], while the application to piezoelectric bonded joints is presented in [1, 2]. Based on the virtual work principle, the eigenvalue equation for computing p is given by:

$$(p^{2}[\mathbf{A}] + p[\mathbf{B}] + [\mathbf{C}])\{\mathbf{u}\} = 0$$
(13)

where [A], [B], and [C] are coefficient matrices defined by the material properties,  $p=1-\lambda$ , and  $\{\mathbf{u}\}$  represents the eigenvector consisting of displacement and electric potential components.

The  $\lambda_n$  at both the vertex and a selected point along the singular line are evaluated. The corresponding angular functions at the vertex are normalized as described by:

$$\begin{cases} f_{\theta\theta v}^{(1)} \left(\frac{\pi}{2}, \frac{\pi}{4}\right) = 1\\ f_{r\phi v}^{(2)} \left(\frac{\pi}{2}, \frac{\pi}{4}\right) = 1\\ f_{\theta\theta v}^{(3)} \left(\frac{\pi}{2}, \frac{\pi}{4}\right) = 1 \end{cases}$$

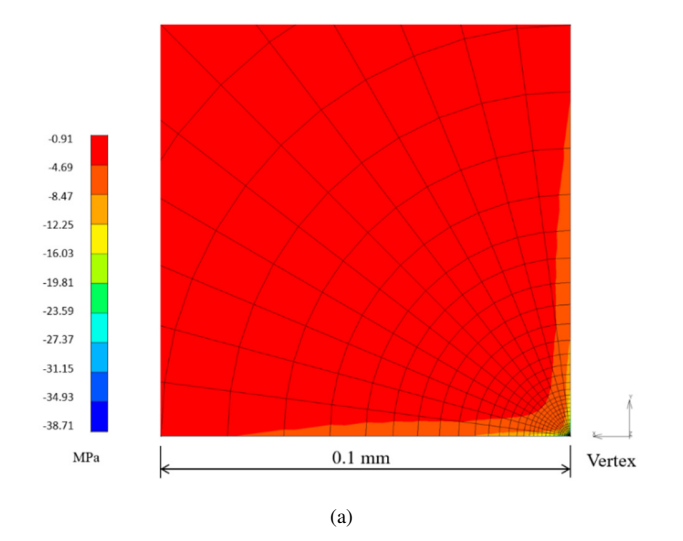
$$(14)$$

At the singular line, the angular functions are normalized under the conditions of :

$$\begin{cases} f_{\theta\theta_l}^{(1)} \left(\frac{\pi}{2}, \frac{\pi}{2}\right) = 1\\ f_{r\theta_l}^{(2)} \left(\frac{\pi}{2}, \frac{\pi}{2}\right) = 1\\ f_{\theta\theta_l}^{(3)} \left(\frac{\pi}{2}, \frac{\pi}{2}\right) = 1 \end{cases}$$

$$(15)$$

The  $\lambda_n$  along with the corresponding angular functions used in this study, are adopted from [7], where a similar geometry and material configuration were considered. The results are listed in Table II.



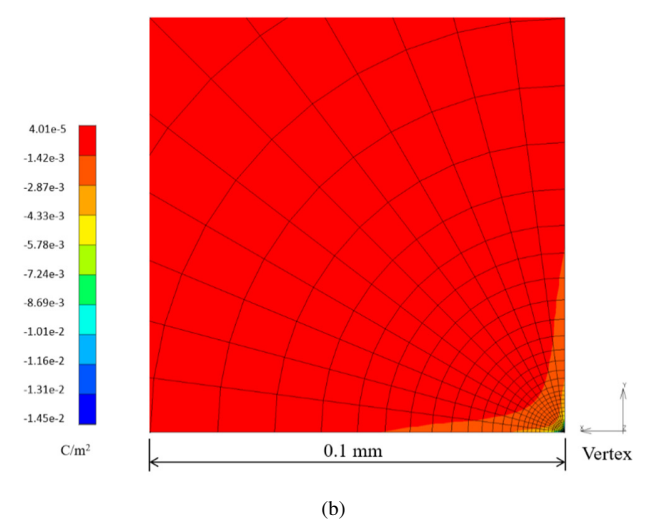


Fig. 2. (a)  $\sigma_{\theta\theta}$  and (b)  $D_{\theta}$  at the interface near the vertex.

TABLE II. THE ORDER OF STRESS SINGULARITIES

	$\lambda_1$	$\lambda_2$	$\lambda_3$
Vertex	0.575	0.211	0.109
Line	0.459	0.324	0.096

#### E. Conservative Integral Method for Intensity Factor Determination

A three-dimensional form of the conservative integral was is formulated in [23], and has been adapted to extract the  $K_n$  factors at both the vertex and along the interface in piezoelectric bonded structures, as shown in [6, 7]. The integral can be expressed in its general form as:

$$\int_{s} (T'_{i}u_{i} - T_{i}u'_{i})ds = 0 \tag{16}$$

Following the methodology of [5, 6], the *H*-integral at the singular location is given by:

$$H = \int_{Sr} (\sigma'_{ij} u_i - \sigma_{ij} u'_i) \hat{n}_j ds \tag{17}$$

where  $S_{\Gamma}$  represents an arbitrarily selected surface enclosing the singular point.

In the present implementation, the integration surface  $S_{\Gamma}$  was defined as a spherical surface of radius r=0.3 mm, centered at the singular point—either at the vertex or a selected location along the interface. This spherical geometry aligns with the radial nature of the singular stress field and simplifies the surface integration process.

The field quantities used in (17), including the stress tensor, displacement, and their corresponding primed values, were extracted from the FEM solution. The resulting H-integral was then used to compute the individual  $K_n$  by exploiting the orthogonality between the angular functions of the singular terms. The complete field expressions, including the primed and unprimed solution sets required to evaluate (17), are derived following the same approach outlined in [5, 6]. The methodology used in this study is consistent with previous works on similar bonded joints [6, 7], where comparable numerical approaches yielded reliable results. These studies serve as a reference supporting the credibility of the present analysis.

#### III. RESULTS AND DISCUSSION

Based on the  $\lambda_n$  presented in Table II, the model exhibits three terms of singularity at both the vertex and the singular line. Accordingly, all three terms are considered in the analysis of intensity factors. These factors are evaluated at the vertex and along the interface line. The intensity factors are evaluated at several points, with a higher sampling density near the vertex to better capture the singularity characteristics.

The stress intensity factors at both the vertex and a point along the singular line are determined using a conservative integral in combination with three-dimensional FEM analysis via MSC Marc software. The FEM models shown in Figure 3 are employed to extract the displacements and electric potentials at the vertex and at an interface location with D/L = 0.15, respectively. The ratio D/L represents the distance between the evaluated point and the vertex normalized by the total interface length. Both models use eight-node brick elements, and the mesh near the singular point is constructed in a spherical pattern centered at the singular point to facilitate the radial integration for the conservative integral. The smallest element in this region has a radial size of 0.01 mm. The vertex model in Figure 3(a) contains 10,872 elements and 11,948

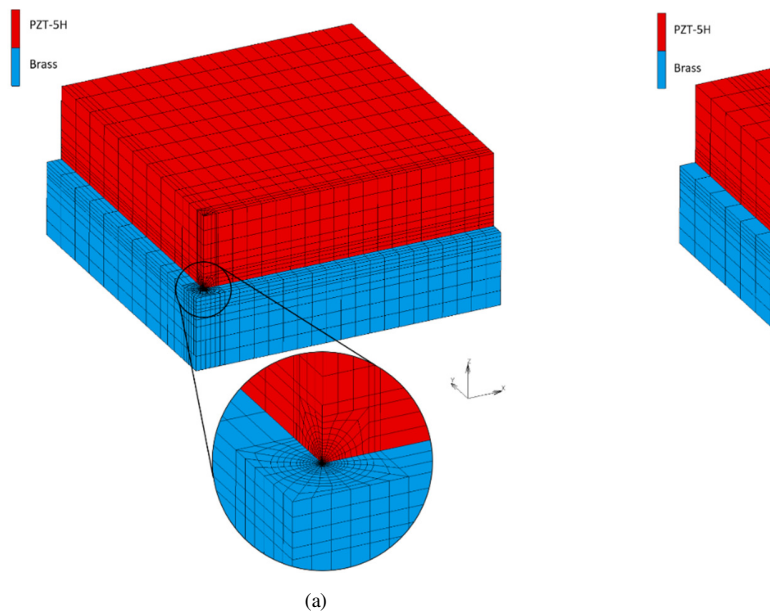
nodes, while the interface model in Figure 3(b) comprises 11,979 elements and 12,926 nodes. All computed results are summarized in Table III and illustrated graphically in Figure 4. It can be seen from Figure 4 that the intensity factor remains relatively constant at positions away from the vertex.

In this study, particular attention is given to the near-vertex region. The results indicate that the three terms of singularity exhibit distinct trends in this region, which differ from the observation in [14] that analyzes the one-real singularity cases, where the interface intensity factor was reported to increase as the point approaches the vertex. In contrast, the present study's results show that only  $K_1$ , which is associated with the highest singularity order, demonstrates a monotonic increase in magnitude, toward a negative value, as the vertex is approached, eventually converging to the  $K_1$  value at the vertex. This indicates that  $K_1$  governs the dominant stress behavior near the bonded corner and is critical in assessing the

failure potential under compressive loading as well as the associated electromechanical response.

TABLE III. THE INTENSITIES OF SINGULARITIES

	D/L	$K_1$	$K_2$	$K_3$
$K_n^{vertex}$	0.000	-258.824	0.725	-457.114
	0.025	-197.487	3.569	-428.853
	0.050	-189.904	0.201	-432.946
	0.075	-186.620	-4.651	-436.674
	0.100	-184.853	-7.740	-441.197
	0.150	-184.925	-10.913	-450.167
$K_n^{line}$	0.200	-186.554	-12.447	-457.897
	0.300	-189.961	-12.895	-468.963
	0.400	-191.392	-11.794	-474.047
	0.500	-190.982	-9.973	-474.833
	0.600	-189.654	-7.842	-473.451
	0.700	-188.161	-5.675	-471.444



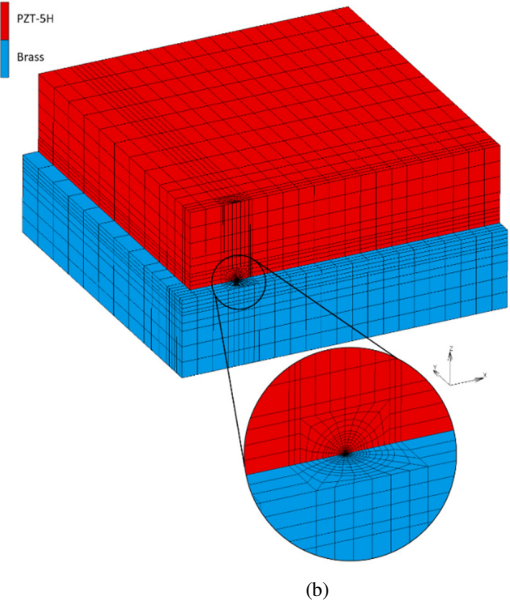


Fig. 3. FEM model constructed to obtain displacement and electric potential fields: (a) in the vertex region and (b) along the singular line at d/L = 0.15.

In comparison, the trends of  $K_2$  and  $K_3$  do not exhibit a consistent or predictable relationship with their respective values at the vertex. Their behaviors are non-monotonic and fluctuate along the interface line. This may be influenced by factors, such as local field interactions, boundary-induced perturbations, or the nature of compressive loading, which may not fully activate shear-related or lower-order singular terms. Nevertheless, the precise mechanisms remain unclear and warrant further investigation.

To validate the results obtained from the proposed calculation, the former are compared against the FEM simulations in which a refined meshing technique is applied in the singular zone to enhance the numerical accuracy. Figures 5 and 6 depict the comparison of the stress component,  $\sigma_{\theta\theta}$ , and the electric displacement,  $D_{\theta}$ , near the vertex. The close agreement between the two approaches confirms the validity of the intensity factor extraction.

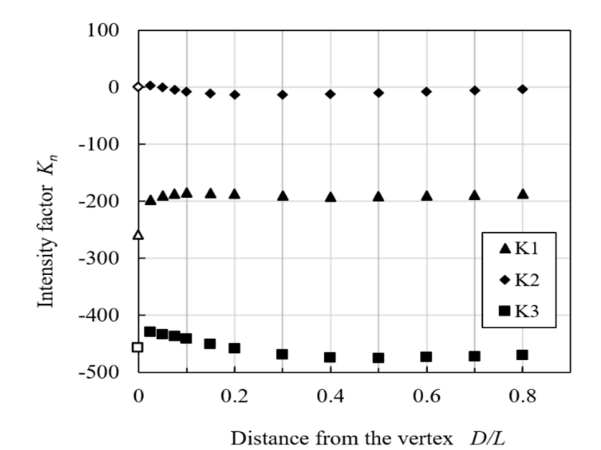


Fig. 4. Variation of intensity factors  $K_1$ ,  $K_2$ , and  $K_3$  along the interface line as a function of the normalized distance from the vertex (D/L).

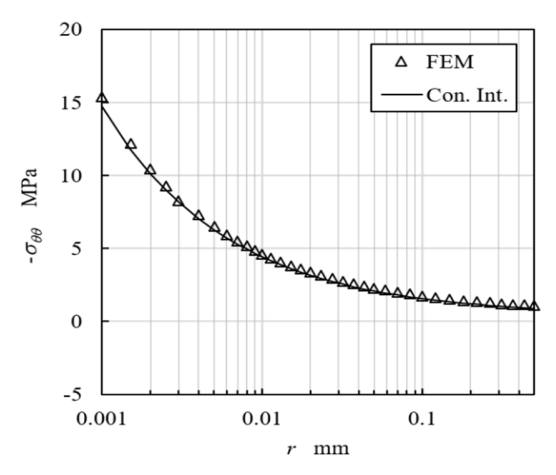


Fig. 5. Distributions of normal stresses at the vertex, at  $\phi = 45^{\circ}$  and  $\theta = 90^{\circ}$ , with respect to r.

For a more detailed insight, the contribution of each singularity term to  $\sigma_{\theta\theta}$  is plotted separately in Figure 7. The first term  $(\sigma_{\theta\theta}(r,\theta,\phi) = K_1\left(\frac{r}{L}\right)^{-\lambda_1} f_{\theta\theta}^{(1)}(\theta,\phi))$  associated with the highest singularity order, governs the behavior near the vertex, which may explain why only  $K_1$  exhibits a significant increase as the vertex is approached. The second term, which corresponds to  $\lambda_2$  and  $K_2$ , contributes values close to zero and has a negligible influence on the overall stress variation. This is likely because  $K_2$  is associated with shear-dominated stress components, which are not prominent under the compressive loading condition. As a result, its contribution remains minimal throughout the interface. Despite having a relatively large intensity factor  $K_3$ , the third term is linked to a small singularity order  $\lambda_3$ , leading to a minimal effect on the stress field, even when approaching the singular point.

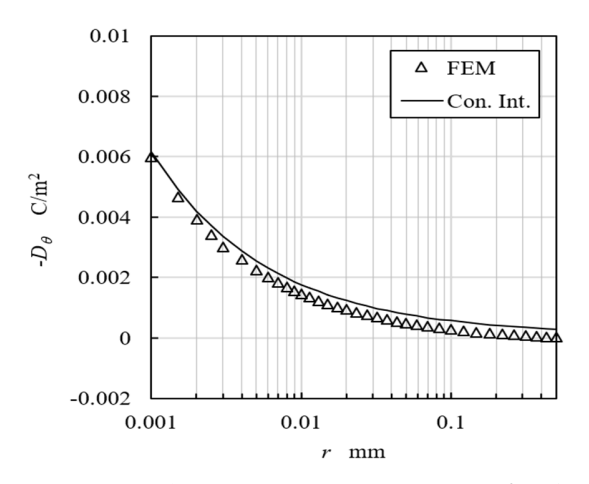


Fig. 6. Distributions of electric displacements at the vertex, at  $\phi = 45^{\circ}$  and  $\theta = 90^{\circ}$ , with respect to r.

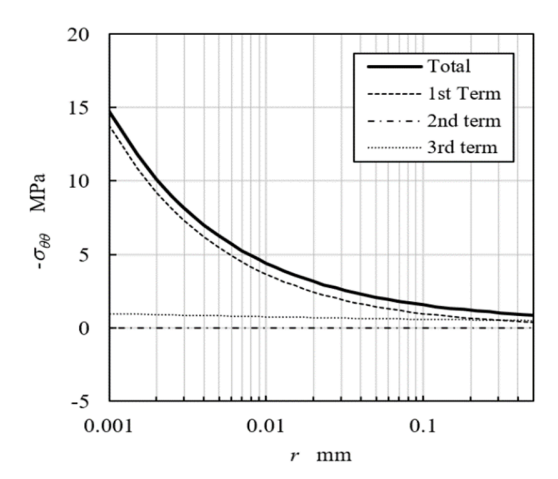


Fig. 7. Distributions of normal stresses at the vertex, at  $\phi = 45^{\circ}$  and  $\theta = 90^{\circ}$ , with respect to r.

#### IV. CONCLUSIONS

This study investigated the behavior of stress intensity factors in a piezoelectric—brass bonded joint under compressive loading, with particular focus on the vicinity of a vertex exhibiting three real singularity terms. The numerical results indicate that the three intensity factors  $K_1$ ,  $K_2$ , and  $K_3$  exhibit distinct and non-uniform trends with distance from the vertex. While  $K_1$  increases consistently and converges to its vertex value,  $K_2$  and  $K_3$  exhibit non-monotonic trends, whose underlying mechanisms remain unclear.

The findings differ from those reported in one-real singularity cases, where the intensity factors along the interface line increase monotonically toward the vertex. The present results highlight the limitations of such assumptions in multisingularity contexts and emphasize the need for more comprehensive models that capture the interaction between multiple singular terms. Therefore, further investigation is required to establish whether a generalizable relationship exists between the singularity intensity along the interface line and that at the vertex in cases involving multiple concurrent singularities. Such insight will be essential for improving the predictive accuracy of singularity-based failure assessments in piezoelectric bonded joints.

### ACKNOWLEDGMENT

This research was supported by Faculty of Engineering Research Fund, Thammasat School of Engineering, Thammasat University.

# REFERENCES

- [1] Md. S. Islam and H. Koguchi, "Analysis of Singularity at a Vertex in 3D Transversely Isotropic Piezoelectric Single-Step Bonded Joints with Various Thicknesses by Boundary Element Method," *Journal of Solid Mechanics and Materials Engineering*, vol. 6, no. 7, pp. 844–859, 2012, https://doi.org/10.1299/jmmp.6.844.
- [2] Md. S. Islam and H. Koguchi, "Characteristics of Singular Stress Distribution at a Vertex in Transversely Isotropic Piezoelectric Dissimilar Material Joints," *Journal of Solid Mechanics and Materials Engineering*, vol. 4, no. 7, pp. 1011–1026, 2010, https://doi.org/10.1299/jmmp.4.1011.

- [3] C.-D. Chen, "On the singularities of the thermo-electro-elastic fields near the apex of a piezoelectric bonded wedge," *International Journal of Solids and Structures*, vol. 43, no. 5, pp. 957–981, Mar. 2006, https://doi.org/10.1016/j.ijsolstr.2005.03.011.
- [4] J.-Q. Xu and Y. Mutoh, "Singularity at the Interface Edge of Bonded Transversely Isotropic Piezoelectric Dissimilar Materials," JSME International Journal Series A Solid Mechanics and Material Engineering, vol. 44, no. 4, pp. 556–566, 2001, https://doi.org/10.1299/jsmea.44.556.
- [5] C. Luangarpa and H. Koguchi, "Evaluation of intensities of singularity at three-dimensional piezoelectric bonded joints using a conservative integral," *European Journal of Mechanics - A/Solids*, vol. 72, pp. 198– 208, Nov. 2018, https://doi.org/10.1016/j.euromechsol.2018.05.012.
- [6] C. Luangarpa and H. Koguchi, "Singular Stresses at a Vertex and Along a Singular Line in Three-dimensional Piezoelectric Bonded Joints," *Journal of Applied and Computational Mechanics*, vol. 6, no. Special Issue, pp. 1364–1370, Dec. 2020, https://doi.org/10.22055/jacm.2020.33956.2379.
- [7] C. Luangarpa, C. Kanchanomai, and H. Koguchi, "Singularities at interface corners of piezoelectric-brass unimorphs," *Journal of the Mechanical Behavior of Materials*, vol. 31, no. 1, pp. 755–766, Jan. 2022, https://doi.org/10.1515/jmbm-2022-0254.
- [8] M. Hrstka, M. Kotoul, T. Profant, and M. Kianicová, "Small-scale domain switching near sharp piezoelectric bi-material notches," *International Journal of Fracture*, vol. 249, no. 2, Mar. 2025, Art. no. 25, https://doi.org/10.1007/s10704-024-00823-1.
- [9] N.-A. Noda and R. Takaki, "Adhesive strength improvement by providing steps in joints and differentiating initial and final debonding stresses," *Materials & Design*, vol. 245, Sept. 2024, Art. no. 113258, https://doi.org/10.1016/j.matdes.2024.113258.
- [10] N.-A. Noda, R. Takaki, Y. Sano, and B. Wang, "ISSF method to evaluate adhesive strength when two distinct singular stress fields appear along the interface," *International Journal of Fracture*, vol. 241, no. 1, pp. 95–114, Feb. 2023, https://doi.org/10.1007/s10704-023-00690-2.
- [11] S. Somadder and S. Islam, "Effect of Adhesive Layer Thickness and Slant Angle on Piezoelectric Bonded Joints," *Journal of Mechanical Engineering*, vol. 19, no. 2, pp. 251–268, Apr. 2022.
- [12] Z. Zhou, Z. Yang, W. Xu, X. Yu, C. Xu, and X. Xu, "Evaluation of electroelastic singularity of finite-size V-notched one-dimensional hexagonal quasicrystalline bimaterials with piezoelectric effect," *Theoretical and Applied Fracture Mechanics*, vol. 100, pp. 139–153, Apr. 2019, https://doi.org/10.1016/j.tafmec.2019.01.003.
- [13] I. Benchadli, M. Benachour, F. Sebaa, and N. Benachour, "Evaluation of Critical Stress Intensity Factor for Different RSW Joints," *Engineering*, *Technology & Applied Science Research*, vol. 14, no. 5, pp. 16766– 16771, Oct. 2024, https://doi.org/10.48084/etasr.8030.
- [14] C. Luangarpa and H. Koguchi, "Analysis of singular stresses at a vertex and along a singular line in three-dimensional bonded joints using a conservative integral," *European Journal of Mechanics - A/Solids*, vol. 60, pp. 208–216, Nov. 2016, https://doi.org/10.1016/j.euromechsol.2016.08.002.
- [15] L. Banks-Sills and A. Sherer, "A conservative integral for determining stress intensity factors of a bimaterial notch," *International Journal of Fracture*, vol. 115, no. 1, pp. 1–25, May 2002, https://doi.org/10.1023/A:1015713829569.
- [16] L. Banks-Sills, "A Conservative Integral for Determining Stress Intensity Factors of a Bimaterial Strip," International Journal of Fracture, vol. 86, no. 4, pp. 385–398, Aug. 1997, https://doi.org/10.1023/A:1007426001582.
- [17] J. P. Dempsey and G. B. Sinclair, "On the singular behavior at the vertex of a bi-material wedge," *Journal of Elasticity*, vol. 11, no. 3, pp. 317– 327, July 1981, https://doi.org/10.1007/BF00041942.
- [18] D. Munz and Y. Y. Yang, "Stress singularities at the interface in bonded dissimilar materials under mechanical and thermal loading," *Journal of Applied Mechanics*, vol. 59, no. 4, Nov. 1992, https://doi.org/10.1115/1.2894053.
- [19] P. Tong, T. H. H. Pian, and S. J. Lasry, "A hybrid-element approach to crack problems in plane elasticity," *International Journal for Numerical*

- *Methods in Engineering*, vol. 7, no. 3, pp. 297–308, Jan. 1973, https://doi.org/10.1002/nme.1620070307.
- [20] S. E. Benzley, "Representation of singularities with isoparametric finite elements," *International Journal for Numerical Methods in Engineering*, vol. 8, no. 3, pp. 537–545, Jan. 1974, https://doi.org/10.1002/nme.1620080310.
- [21] S. S. Pageau and S. B. Biggers, "Finite element evaluation of free-edge singular stress fields in anisotropic materials," *International Journal for Numerical Methods in Engineering*, vol. 38, no. 13, pp. 2225–2239, July 1995, https://doi.org/10.1002/nme.1620381306.
- [22] T. Ikeda, Fundamentals of Piezoelectricity. Oxford, UK: Oxford University Press, 1990.
- [23] C. Luangarpa and H. Koguchi, "Analysis of a three-dimensional dissimilar material joint with one real singularity using a conservative integral," *International Journal of Solids and Structures*, vol. 51, no. 15, pp. 2908–2919, Aug. 2014, https://doi.org/10.1016/j.ijsolstr.2014.04.018.